Journal of Fluids and Structures (1998) **12,** 703–716
Article No. fl980166

EXPERIMENTAL AND NUMERICAL INVESTIGATION OF 2-D BACKWARD-FACING STEP FLOW

T. Lee and D. Mateescu

Department of Mechanical Engineering, McGill University, Montreal, Québec, Canada

(Received 21 July 1997 and in revised form 8 May 1998)

Results of experimental and numerical investigations of air flows over a two-dimensional backward-facing step are presented. The lengths of separation and reattachment on the upper and lower walls were measured nonintrusively using closely spaced, multi-element hot-film sensor arrays for $Re \leq 3000$ and expansion ratios of 1·17 and 2·0. The hot-film sensor measurements are in good agreement with the present as well as previous numerical predictions. It is anticipated that this measurement capability will provide a practical means for the study of unsteady flow phenomena with flow separation as well.

1. INTRODUCTION

The separation of the flow and its subsequent reattachment to a solid surface occurs in many systems, and is of practical as well as of theoretical interest. Some examples of these applications are flows over airfoils at large angles of attack, in a channel whose area suddenly increases, and in gas turbines and heat transfer devices. The location of the reattachment zone and its flow structure also determine the local heat and mass transport properties of the flow. The importance of such flows to engineering equipment has been stressed in many publications [see e.g. Abbott and Kline (1962), Goldstein *et al.* (1970), and Eaton and Johnston (1981)], and attempts have been made to develop advanced experimental and theoretical techniques in order to study the flows with separation regions. However, due to the complexity of the flow behaviour associated with the flow separation and reattachment, the numerical and experimental methods capable of accurately characterizing these flow features are still far from perfect.

In order to obtain a better understanding, either numerically or experimentally, of the complex fluid flow following separation and including reattachment, the two-dimensional flow past a backward-facing step is a standard test problem as well as a building-block flow for workers developing turbulence models, and it has been addressed by numerous authors using a variety of numerical and experimental methods (Goldstein *et al.* 1970; Hussain and Reynolds 1975; Westphal *et al.* 1981; Eaton *et al.* 1981; Armaly *et al.* 1983; Westphal and Johnston 1984; Vogel and Eaton 1985; Adams and Johnston 1988; Gartling 1990; Mateescu *et al.* 1994). The basic flow situation is shown in Figure 1(a). Fluid flows with an average velocity, U, past a step of height H with channel heights upstream and downstream of the step represented by H_u and H_d, respectively. After the flow separates at the step, the flow reattaches to the lower wall at a distance x_r. However, even with modern calculation methods, the reattachment distance is still underpredicted, and the predictions of the flow field become worse as the flow proceeds into the recovery region [see e.g., Adams and Johnston (1988)]. Indeed, it is hard to imagine a successful prediction of either the separation zone or the flow downstream of reattachment, if the reattachment length and

0889–9746/98/060703 + 14 $30.00

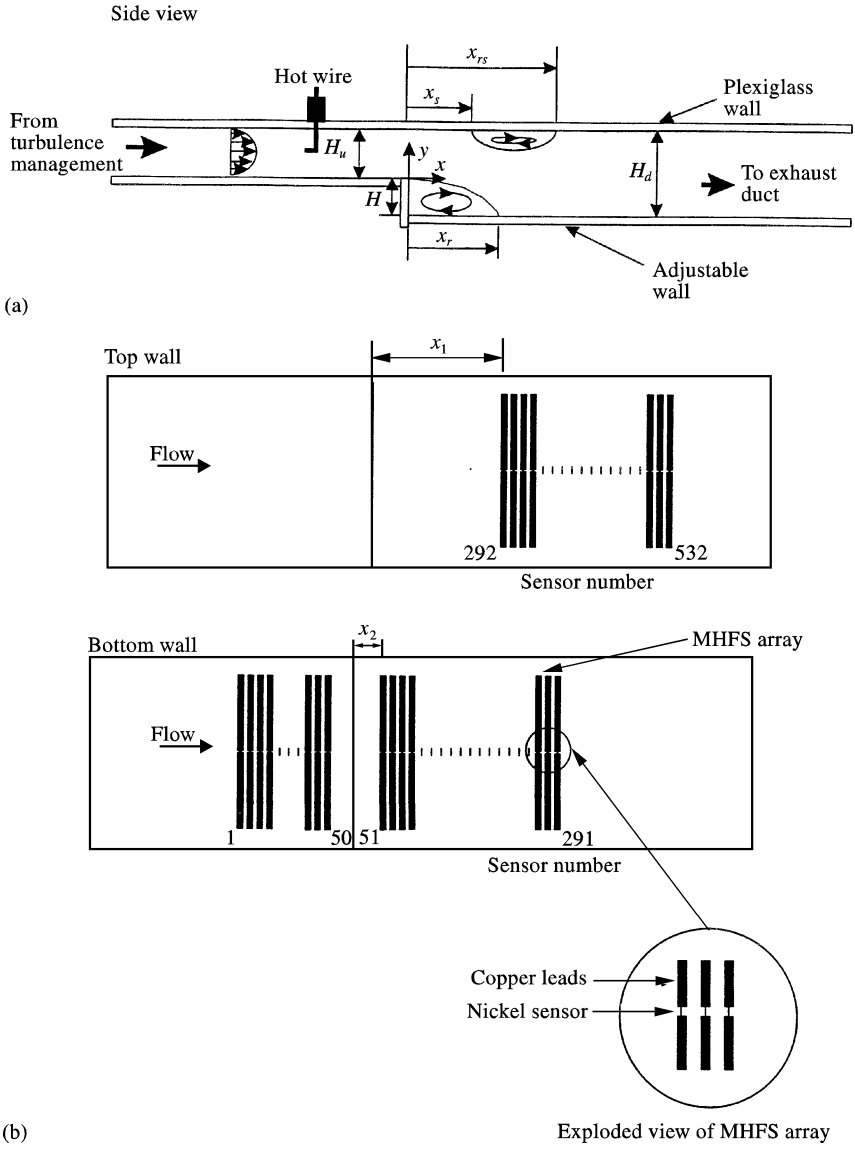

Figure 1. Schematic illustration of (a) air tunnel and geometry of backward-facing flowfield, and (b) the multi-element hot-film sensor array ($x_1 = 92$ mm and $x_2 = 13{\cdot}5$ mm).

structure in the reattachment zone are incorrectly predicted. Therefore, it is important to supply data which can be used to validate the numerical codes and may aid the development of future models.

However, due to the presence of a reversing flow, conventional surface pressure measurement and hot-wire arrays cannot conveniently be used in this region. Recently, laser-Doppler velocimetry with frequency shifting (Armaly *et al.* 1983), wall-flow-direction probes (Eaton *et al.* 1979; Adams & Johnston 1988), and qualitative smoke-wire flow visualization methods (Goldstein *et al.* 1970) have been used to obtain the reattachment length downstream of a backward-facing step flow. However, these techniques are either

too complicated and expensive, or have the disadvantage of requiring knowledge of the location of the reattachment location beforehand. Furthermore, due to the different measurement techniques and flow facilities used, there is a scatter in the existing data sets of reattachment lengths (Adams & Johnston 1988). A practical means capable of detecting nonintrusively the locations of the reattachment and separation points would certainly be advantageous.

The objective of this study was to measure nonintrusively the locations of the reattachment and separation points for fully developed laminar and transitional channel flows over a two-dimensional backward-facing step using the closely spaced, multi-element hot-film sensor (MHFS) arrays, in conjunction with a bank of constant-temperature anemometers. Hot-wire velocity measurements were also made to supplement the MHFS measurements. Numerical predictions of the flow reattachment and separation points were also undertaken by the authors, and comparisons of the predictions and measurements are presented in this paper.

2. EXPERIMENTAL APPARATUS AND PROCEDURES

2.1. Flow Facility

The small air tunnel with an aspect ratio (width over height) of 40, built for the present experiment, is shown schematically in Figure 1(a). It incorporated a two-dimensional backward-facing step with an adjustable step height (H). The expansion ratio ER $= H_d/H_u$ (where H_u and $H_d = H_u + H$ are the heights of the channel upstream and downstream of the step, respectively) tested was 1·17 and 2·0. The origin of the coordinate system is centered at the step corner. The rectangular test-section was constructed from Plexiglas. The inlet flow passed through a section with flow straighteners and was afterwards guided into a smooth contraction section with a contraction ratio of 20. The outlet of the contraction nozzle was connected to the inlet of the upstream channel test-section, which was 1·2 m in length, and $H_u = 1{\cdot}5$ cm and $W = 60$ cm in height and width, respectively, and with an aspect ratio (W/H_u) of 40 up to the backward-facing step. These dimensions ensured a fully developed laminar flow upstream of the step, characterized by a Reynolds number, Re ($= UH_d/\nu$ where U is the average cross-section velocity, and ν the kinematic viscosity of air) up to 1150. The transitional flow regime for Re between 1150 and 3000 was also investigated.

2.2. Hot-Wire Anemometry

Both the spanwise and transverse velocity profiles at $x = -5$ cm were measured by a hot-wire probe (DISA 55P04) with a constant-temperature anemometer (Dantec model 55C17). The overheat ratio was set at 1·3 so as to minimize the heat conduction loss to the Plexiglas wall (Bhatia *et al.* 1982; Turan & Azad 1987). All hot-wire calibrations, mean-flow measurements, free-stream turbulence levels, r.m.s. disturbance measurements, and subsequent processing were performed using a 486 PC with a 330 kHz A/D converter board (ComputerBoards model Das16/330), and the Streamer data acquisition software. Waveforms and spectral analyses of the u-component velocity fluctuations were also made with an FFT analyzer (HP 3584A). The hot-wire signals were sampled at 2 kHz with a cut-off of 500 Hz. The position of the hot-wire probe was determined using a cathetometer.

The low-speed (0·15–1·1 m/s) hot-wire calibration was performed in a 3 ft $\times$ 2 ft subsonic wind tunnel by using the vortex-shedding method suggested by Lee & Budwig (1991). By positioning a hot-wire probe in the laminar wake of a steel wire of a diameter $d = 4{\cdot}5$ mm, the free-stream velocity, U, was extracted directly

from the frequency of vortex shedding, f_S, measured with a HP 3485A FFT analyzer, using the Strouhal number–Reynolds number (St–Re_d) relationship, $St = f_S d/U = 0{\cdot}212 - 4{\cdot}5/Re_d$, for a Reynolds number, $Re_d = Ud/v$, based on the wire diameter between 50 and 150. A fourth-order polynomial was fitted to the velocity–voltage calibration points using a least-squares approximation. The calibration before and after each test run was reproduced to within 2% of each other.

2.3. Multi-Element Hot-Film Sensor (MHFS) Array

The MHFS array used in the present experiment consists of a number of thin nickel films (0·2 μm), which are electron-beam evaporated onto a thin polyimide substrate (50 μm) in a straight-line array. Each sensor consists of a nickel film, 2·5 mm long and 0·1 mm wide, with 10 μm copper-coated nickel leads routed to provide wire attachment away from the measurement location. The nominal resistance of the sensor is 20 Ω. The entire sensor array consists of 291 sensors (S_1-S_{291}) on the lower wall and 240 (S_{292}-S_{532}) on the upper wall. The sensors are spaced at $S = 1{\cdot}25$ mm apart. The sensor arrays were bonded onto the Plexiglas walls using nonconducting, double-sided mylar adhesive, which prevented the sensor array from introducing surface irregularities to the channel surface. The sensor pattern and the layout of the leads are shown in Figure 1(b).

Groups of 14 of the 532 sensors in total were systematically connected to 14 constant-temperature anemometers (AA Lab System model AN-2000) to obtain both time history and spectral information at each sensor position. The sensors were connected to the constant-temperature anemometers (CTAs) using magnet wire (0·1 mm diameter) and BNC coaxial cable combination to minimize the disturbance to the flow in the tunnel test-section. The overheat ratio was set at 1·09, which ensures that only a small amount of heat was introduced, and the heated thin films caused little disturbance to the shear layer or to each other. This was checked by heating the films individually and in groups while monitoring the effects on other films. The hot-film sensors were uncalibrated and the overheat and offset voltages for each sensor was carefully adjusted such that each sensor was at nearly the same operating conditions. The fluctuating voltage output of the CTA also represents a function of the dynamic shear stress present at each hot-film sensor location. CTA output signals were sampled at 2 kHz and low-pass filtered (with a cutoff of 500 Hz) and amplified by a gain between 50 and 100. Special care must be taken when high values of feedback gains of the CTAs were used (it is necessary when the hot-film signal levels fall to very low values) which could lead to system instabilities in balancing the Wheatstone bridge circuit. The signals from sensor S_{28}, located at $x = -3{\cdot}8$ cm upstream of the step, were also recorded to provide reference signals between each set of CTA output signals. The amplified signals were also connected to a four-channel oscilloscope (LeCroy model 9304) to provide on-line time history traces of the operating group of sensors.

No calibration of the MHFS was needed as the objective of this study was not to determine the magnitude of the wall shear stress, but rather to study the simultaneous output signals of the MHFS qualitatively, i.e. to detect the locations of the flow separation and reattachment points. It is worth noting that the qualitative extraction of the state of the boundary layer also relieves the great difficulty encountered in the calibrating of multiple surface-mounted hot-film sensors (Lorber *et al.* 1992). These difficulties are attributed to the need to (i) calibrate all probes in a reference unsteady flow before installation, (ii) provide a reference flow at each sensor, or (iii) calibrate the sensors by comparison to a traceable and portable reference probe. The other constraint in the use of surface-mounted hot-film sensors, i.e. the influence of nonnegligible heat transfer through polyimide substrate to the model and the fluid, which has been found to be significant in quantitative measurements in

air flow [e.g., Alfredsson *et al.* 1988; Diller & Telionis 1989; Cook 1991], was not believed to be a significant problem in the present method. Detailed descriptions of the MHFS arrays and their functions are given by Lee & Basu (1997).

3. NUMERICAL METHOD

The numerical method used in the present computations is based on a finite difference formulation and uses an artificial compressibility approach (Mateescu *et al.* 1994). Thus, an iterative pseudo-time-integration procedure is used for the solution of the incompressible Navier–Stokes and continuity equations, augmented by an artificial compressibility, which can be expressed in nondimensional conservation-law form as

$$\frac{\partial u^*}{\partial t} + \frac{\partial (u^* u^*)}{\partial x^*} + \frac{\partial (u^* v^*)}{\partial y^*} + \frac{\partial p^*}{\partial x^*} = \frac{1}{\mathrm{Re}} \nabla^2 u^*, \tag{1}$$

$$\frac{\partial v^*}{\partial t} + \frac{\partial (u^* v^*)}{\partial x^*} + \frac{\partial (v^* v^*)}{\partial y^*} + \frac{\partial p^*}{\partial y^*} = \frac{1}{\mathrm{Re}} \nabla^2 v^*, \tag{2}$$

$$\delta \frac{\partial p^*}{\partial t} + \frac{\partial u^*}{\partial x^*} + \frac{\partial v^*}{\partial y^*} = 0, \tag{3}$$

where ∇^2 denotes the Laplace operator defined as $\nabla^2 f = \partial^2 f / \partial x^{*2} + \partial^2 f / \partial y^{*2}$, $x^* = x/H_d$ and $y^* = y/H_d$ are nondimensional Cartesian coordinates, $u^* = u/U$, $v^* = v/U$, $p^* = p/(\rho U^2)$ are the nondimensional velocity components and pressure, and δ is the artificially added compressibility.

An implicit Euler scheme is used to semi-discretize equations (1)–(3) in pseudo-time in the form

$$u^{n+1} + \Delta t \left[\frac{\partial (u^{n+1} u^{n+1})}{\partial x^*} + \frac{\partial (u^{n+1} v^{n+1})}{\partial y^*} + \frac{\partial p^{n+1}}{\partial x^*} - \frac{1}{\mathrm{Re}} \nabla^2 u^{n+1} \right] = u^n, \tag{4}$$

$$v^{n+1} + \Delta t \left[\frac{\partial (u^{n+1} v^{n+1})}{\partial x^*} + \frac{\partial (v^{n+1} v^{n+1})}{\partial y^*} + \frac{\partial p^{n+1}}{\partial y^*} - \frac{1}{\mathrm{Re}} \nabla^2 v^{n+1} \right] = v^n, \tag{5}$$

$$p^{n+1} + \frac{\Delta t}{\delta} \left[\frac{\partial u^{n+1}}{\partial x^*} + \frac{\partial v^{n+1}}{\partial y^*} \right] = p^n, \tag{6}$$

where the subscripts n and $n+1$ denote the values of u^*, v^* and p^* at the pseudo-time level t_n and t_{n+1}, respectively. The spatial discretization of these equations is based on a central difference scheme using a stretched staggered grid.

A factored Alternating Direction Implicit (ADI) scheme is then used to separate the corresponding equations in delta form in two successive sweeps in x^* and y^*. Finally, a special decoupling procedure, based on the utilization of the continuity equation to eliminate the pressure from the corresponding Navier–Stokes equations in each sweep, is used to reduce the problem to the efficient solution of two sets of scalar tridiagonal equations. Details of this computational method can be found in Mateescu *et al.* (1994). A fully developed laminar flow was assumed at the inlet above the step, as in the previous numerical investigations performed by Gartling (1990), Kim and Moin (1985) and Sohn (1988). No-slip boundary conditions were applied at the solid walls, whereas at the outlet the velocity components were extrapolated to second-order accuracy from inside the computational domain. The outlet pressure was obtained by integrating the normal

momentum equation from the bottom wall (Mateescu *et al.* 1994), and in the final solution the pressure level is adjusted to zero at the step corner. The computational domain had a nondimensional length of 30 (based on the downstream height of the channel, H_d) with 500×50 grid points in the x- and y-directions, respectively; the mesh spacing in the x-direction was minimum at the step, $\Delta x_{\min} = 0{\cdot}08$, and maximum at the outlet, $\Delta x_{\max} = 0{\cdot}21$, while in the y-direction the minimum mesh spacing was at the walls, $\Delta y_{\min} = 0{\cdot}015$. Computations were also performed with two coarser grids, showing that the results obtained for the finer grid became almost independent at the mesh size. The converged solutions, when all of the r.m.s. residuals were less than 5×10^{-5}, were obtained for 500×50 grid points in 1·4 h of computing time on a personal computer (fitted with an Alacron i860 board).

4. RESULTS AND DISCUSSION

The two-dimensional character of the flow in the upstream of the backward-facing step with ER = 2·0 was confirmed by hot-wire measurements for various Reynolds numbers (see Figure 2). The hot-wire probe was located at $y = H_u/2$ and $x = -5$ cm. Figure 2 shows that the inlet flow was uniform within 2% over the central portion of 50 cm of its width.

The dimensionless mean velocity profiles, $u(y)/U$ both upstream and downstream of the step with ER = 2·0, at $x = -5$, 21, and 45 cm, respectively, for different Reynolds numbers are shown in Figure 3. Figure 3(a) shows that in the laminar range (Re < 1150), the velocity flow field is close to that of a fully developed laminar channel flow with a slight deviation from a parabolic profile (which may be caused by the pressure change downstream of the sudden expansion). The measured fully developed laminar velocity profiles are consistent with the theoretical results (solid line). The corresponding velocity profiles (solid circles and squares) measured at $x = 21$ cm and 45 cm downstream of the step are shown in Figure 3(b), and they are in good agreement with the present computational results as well with those of Gartling (1990). However, due to the presence of the separated flow region in the vicinity of $x = 21$ cm on the upper wall (as shown in Figures 4 and 7 that follow), no reliable hot-wire measurements were obtained for $0{\cdot}3 < y/H_d < 0{\cdot}5$.

Figure 4(a,b,c) shows three typical composite plots of simultaneously recorded MHFS output signals for Re = 805 and ER = 2·0. The y-axis represents the voltage output level of each sensor. This figure reveals that, even in a visual comparison, there is a 180° phase shift

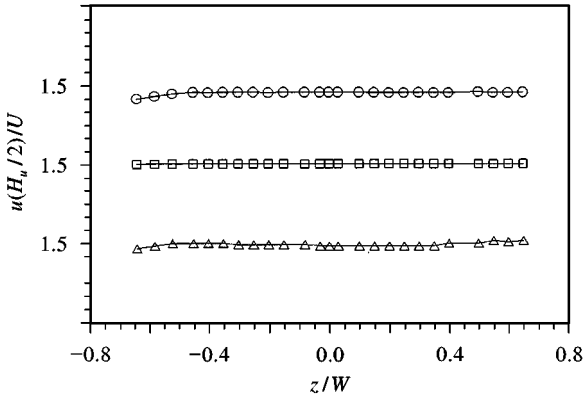

Figure 2. Spanwise mean velocity distributions of the inlet flow with ER = 2·0 for different Re at $x = -5$ cm. ○ Re = 685; □, Re = 805; △, Re = 985.

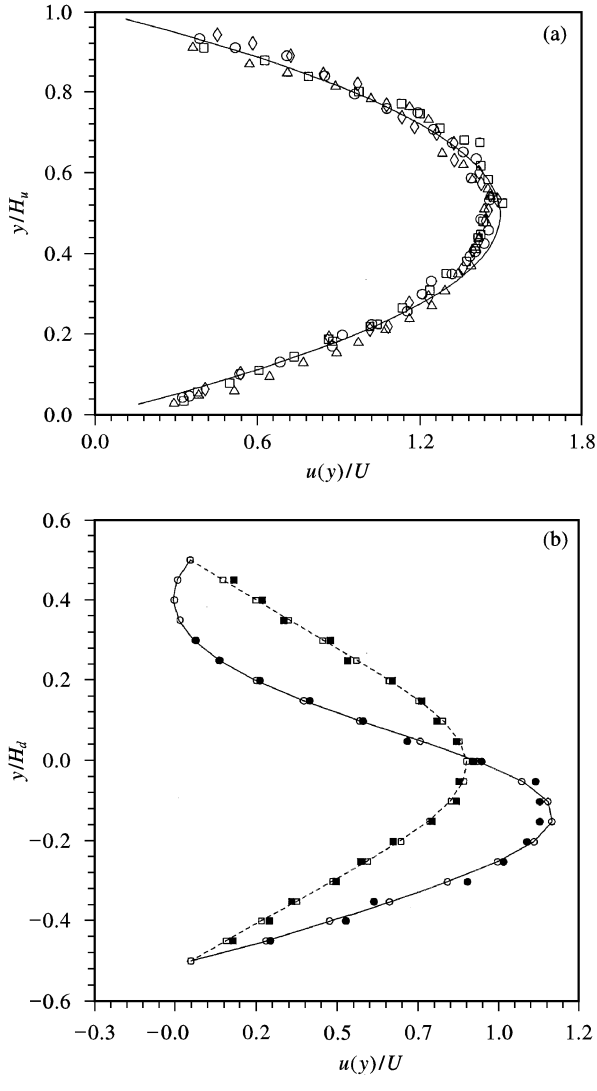

Figure 3. Dimensionless mean velocity profiles for different Reynolds numbers. (a) At $x = -5$ cm. Hot-wire measurements: ○ Re = 475; □, Re = 685; △, Re = 805; ◇, Re = 985; ——, theoretical curve. (b) At $x = 21$ cm: ●, hot-wire measurements for Re = 805; —, present predictions for Re = 800; ○ Gartling (1990) for Re = 800. At $x = 45$ cm: ■, hot-wire measurements for Re = 805; - - - -, present prediction for Re = 800; □, Gartling (1990) for Re = 800.

between the time-trace signals of sensors S_{194} and S_{195} [Figure 4(a)], which allows the determination of the reattachment of the separated shear layer at around sensor S_{194}, i.e., a reattachment length (x_r) of $6{\cdot}45H_d$ on the lower wall. The 180° out-of-phase phenomenon, due to the presence of flow bifurcation at the flow separation point, was first used by Stack *et al.* (1987) and recently by Nakayama *et al.* (1994) to measure the laminar separation bubbles on airfoils, as well as by Lee & Basu (1997) to examine the behaviour of the boundary layer developed on the surfaces of circular cylinders. The presence of the 180° phase shift in the shear stress signals recorded simultaneously upstream and downstream of the separation point on the upper wall can be interpreted as follows. The shear layer

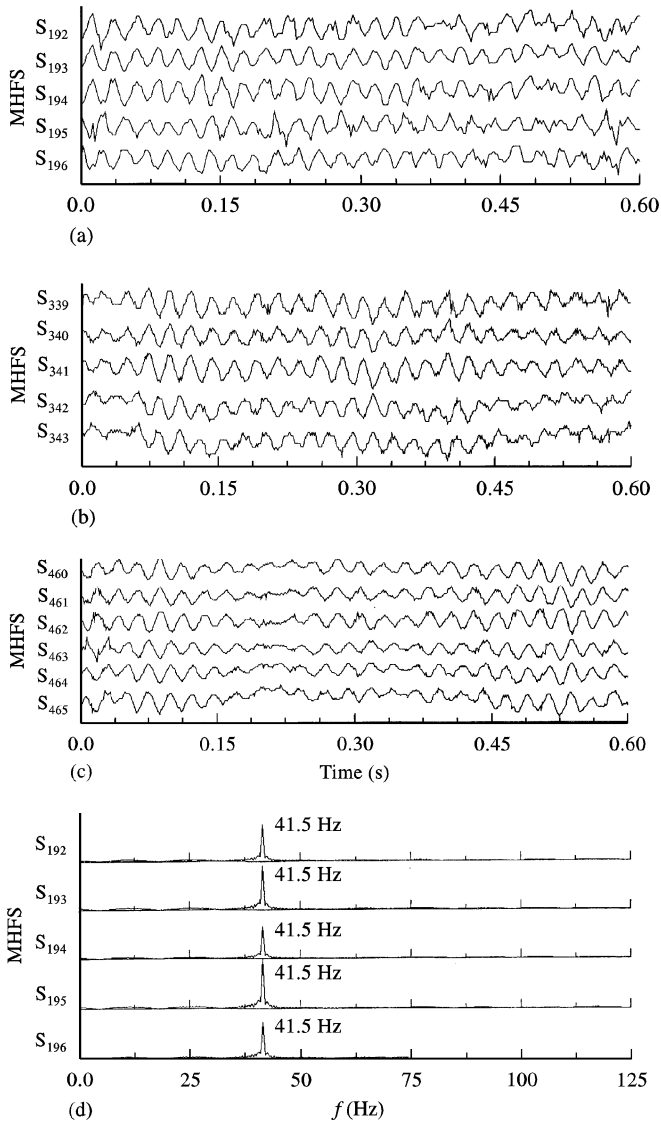

Figure 4. Typical composite plots of simultaneously obtained time-voltage output signals and spectral contents from selected MHFS for Re = 805 and ER = 2. (a) S_{191}-S_{196} across the reattachment on the lower wall; (b) S_{339}-S_{343} across the separation point on the upper wall; (c) S_{460}-S_{465} across the reattachment point on the upper wall; and (d) spectral contents of (a). Note the existence of a 180° phase shift between sensors S_{194} and S_{195}, S_{341} and S_{342}, and S_{462} and S_{463}.

between the separation bubble and the core flow is unstable due to Helmholtz instabilities. For sufficiently high Reynolds numbers, the length of this shear layer is sufficient for these instabilities to grow noticeably, resulting in transverse oscillations of the separating streamline. Since the reattachment point forms the end-points, its position will undergo streamwise oscillations as observed by Cherdron *et al.* (1978). If these oscillations are small enough, then the flow field in the vicinity of the separation can be decomposed into the mean flow and small variations due to the moving separating streamline. The mean shear stresses upstream and downstream of the separation point are directed in the upstream and

downstream direction, respectively, which results in the above-observed 180° phase shift phenomenon. Furthermore, since at the point of reattachment (on the bottom wall), the dividing streamline attaches to the body, the presence of flow bifurcation also allows the identification of the location of the boundary-layer reattachment point. Similarly, the locations of separation point, $x_s = 5{\cdot}15H_d$, across sensors S_{341} and S_{342} [Figure 4(b)], and reattachment point, $x_{rs} = 10{\cdot}25H_d$, across sensor S_{462} and S_{463} [Figure 4(c)] on the upper wall could be obtained.

It is worth noting that the unsteadiness shown in the sensor outputs [Figure 4(b,c)] were due to the system instabilities when high values of gain settings of the CTAs were used. However, this unsteadiness/instability should not affect the qualitative extraction of the locations of separation and reattachment based on the 180° phase shift phenomenon. Figure 4(d) shows the spectral contents of the simultaneously recorded MHFS signals presented in Figure 4(a), which reveals the existence of a dominant characteristic frequency of 41·5 Hz of the boundary layer. It is also worth noting that, even though the MHFS measurements of the locations of laminar separation and reattachment points were successful, the detection of turbulent separation and reattachment was found to be unsatisfactory. The reason for the latter could be due to the strong spanwise motion in the turbulent boundary layer and that much of it is correlated. The above MHFS measurements of x_r, x_s and x_{rs} are consistent with the behaviour of the wall-shear stresses along the upper (solid line) and lower (dashed line) walls [Figure 5(a)], and with the contour plots for the axial (u) and cross-flow (v) components [Figure 5(b,c)] predicted by the computational results.

The presence of a phase difference of 180° in the simultaneously acquired MHFS signals (as shown in Figure 4) can also be confirmed by cross-correlating the hot-film sensor signals across the points of interest (Figure 6). It was found that the MHFS output signals are in-phase upstream of the laminar separation point (indicated by the dotted line across S_{339} and S_{341}), out-of-phase by nearly $+180°$ (indicated by the solid line) and 180° (indicated by the short dash line across reattachment (between S_{462} and S_{463}) and separation (between S_{341} and S_{342}) points on the upper wall, respectively, and out-of-phase of 180° across the reattachment (between S_{194} and S_{195}) on the lower wall (the long-dash line). However, it is worth noting that, even though the MHFS measurements of the locations of laminar separation bubble and reattachment were successful, the detection of turbulent separation and reattachment was not satisfactory. The reason could be because (i) the turbulent velocity fluctuations swamp the shear stress fluctuations due to the moving re-attachment point and/or (ii) the motion of the reattachment point loses its periodicity.

Figure 7 summarizes the MHFS measurements of x_r, x_s, and x_{rs} on the upper and lower walls for $Re \leq 3000$, covering laminar and transitional regimes of the flow, and ER = 2. This figure indicates that for the laminar regime of the flow, the reattachment length (x_r) on the lower wall increases linearly with Re. Also, due to the adverse pressure gradient created by the sudden expansion, a recirculating-flow region (x_{rs} - x_s) was also observed on the upper wall opposite to the step, which initially increased and then decreased in size with increasing Re. The length of x_r decreased sharply followed by a continued gradual reduction for the transitional regime of the flow. The above observations are, in general, consistent with the detailed LDV measurements of Armaly *et al.* (1983) for an ER of 1·94. However, there exists a discrepancy of about 8% between the present MHFS measurements and the LDV data (Table 1). Furthermore, the additional recirculating-flow region on the lower wall reported by Armaly *et al.* was not observed in the present MHFS measurements at Re = 805. In summary, Figure 7 together with Figure 4 indicates that, by the using of MHFS array operated with a bank of CTAs, the locations of the laminar flow separation

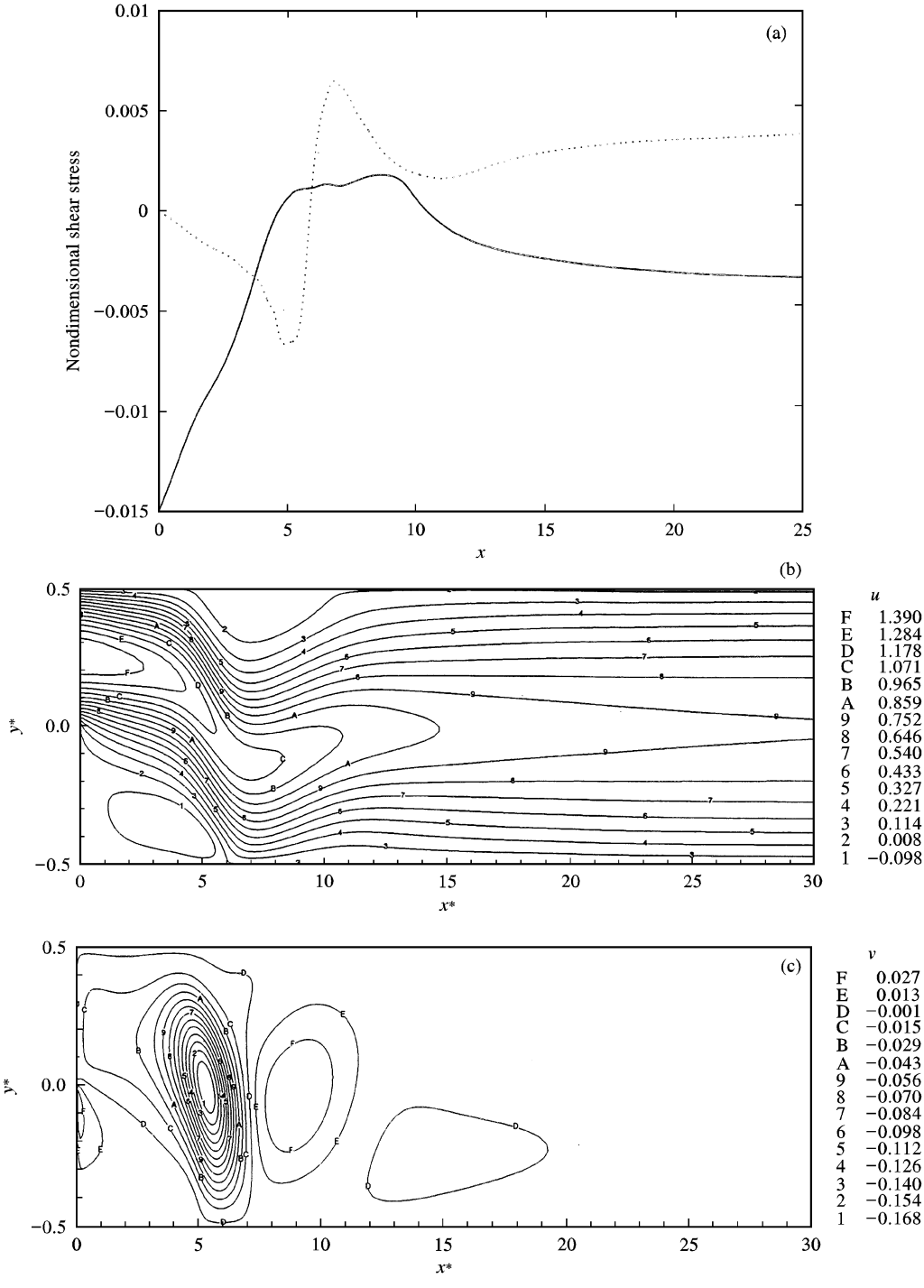

Figure 5. (a) Predicted dimensionless wall-shear stress distribution along the upper and lower walls: ——, upper wall; - - - -, lower wall; (b) predicted u-component contour plot; and (c) predicted v-component contour plot.

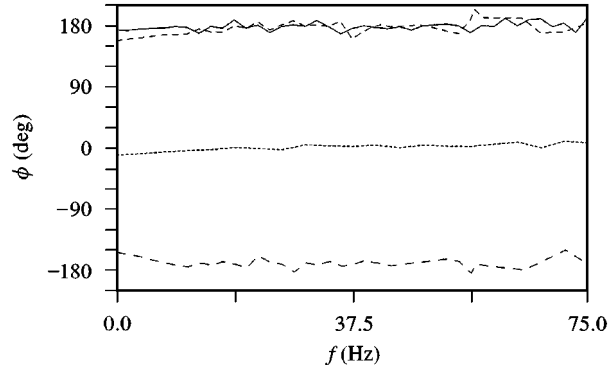

Figure 6. Phase angle of the MHFS signals shown in Figure 4: ....., in phase (S_{339} and S_{341}); ——, $+180°$ out-of-phase (S_{462} and S_{463}); ----, $-180°$ out-of-phase (S_{341} and S_{342}); – – –, $+180°$ out-of-phase (S_{194} and S_{195}).

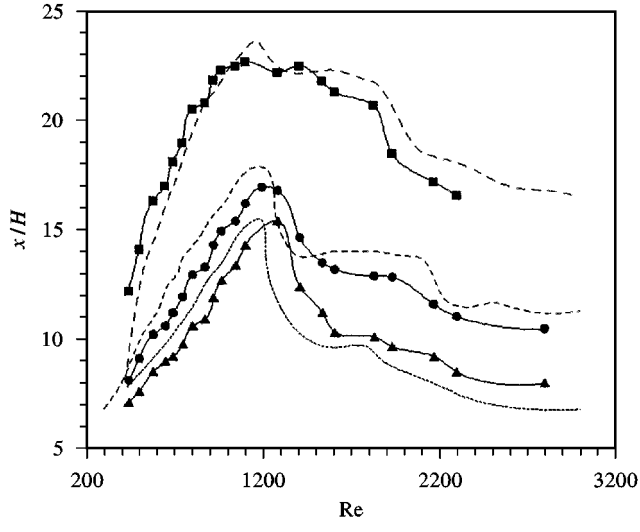

Figure 7. Variation of location of reattachment and separation points, and length of recirculating region on upper and lower walls with Reynolds number for ER = 2. Armaly *et al.* (1983) data: ----, x_r; - - - -, x_s; ....., x_{rs}. MHFS measurements: ●, x_r; ■, x_{rs}; ▲, x_s.

and reattachment points in a 2-D backward-facing flow can be measured both nonintrusively and simultaneously. The maximum experimental uncertainty associated with the MHFS measurements presented in Figures 4 and 7 is within $S/x_r\% = 1{\cdot}25/6{\cdot}45H_d\% = 0{\cdot}6\%$ for ER = 2 (where $S = 1{\cdot}25$ mm is the sensor spacing).

The effect of the expansion ratio, ER, on the variation of x_r was also examined by performing experiments for ER = 1·17. The results obtained are compared in Figure 8 with those of Armaly *et al.* (1983) and Goldstein *et al.* (1970). Figure 8 indicates that there is no scatter in both the present MHFS measurements and the Armaly *et al.* LDV data, and that, similar to the case of ER = 2·0, x_r increases linearly with the Reynolds number (in this case based on the step height, $Re_H = UH/\nu$) in the laminar flow regime, but at a slower rate.

TABLE 1
Comparison of computed predictions and experimental measurements of dimensionless lengths (with respect to H_d) of separation and reattachment on the upper and lower walls

Length on		Experimental results		Computed results*			
		Present MHFS data†	LDV data (Armaly *et al.* 1983)‡	Present prediction	Gartling's prediction (1990)	Kim & Moin (1985)	Sohn (1988)
Lower wall	x_r	6·45	7.0	6·0	6·1	6·0	5·8
	x_s	5·15	5·7	4·80	4·85	—	—
Upper wall	x_{rs}	10·25	10·0	10·30	10·48	—	—
	$x_{rs} - x_s$	5·1	4·3	5·50	5·63	5·75	4·63

*ER = 2 and Re = 800; †ER = 2 and Re = 805; ‡ER = 1·94 and Re = 800

The present experimental results obtained for the flow separation and reattachment locations on the upper and lower walls, x_r, x_{rs}, x_s, and x_{rs} - x_s, for Re = 805 and ER = 2, are compared in Table 1 with the present numerical predictions for Re = 800, as well as with the results obtained by Gartling (1990), Kim and Moin (1985) and Sohn (1988), using different numerical methods, and with the LDV data obtained by Armaly *et al.* (1983). The numerical results shown in Table 1 were computed disregarding the upstream portion of the channel and considering a fully developed laminar flow just upstream of the backstep, in order to have a consistent validation against the benchmark solution provided by Gartling (1990). Thus, a fully developed velocity profile defined by the velocity components $u = 24y(0{\cdot}5 - y)U$ and $v = 0$ was assumed at the inlet ($x = 0$) above the step. It is also worth noting that the converged solutions were obtained for 500×50 grid points in 1·4 h of computing time on a personal computer (fitted with an Alacron i860 board), while Gartling's benchmark solutions were obtained using a finite-element method with 0·2 h per iteration on a CRAY XMP/416 for 400×20 elements with nine nodes. The comparison given in Table 1 shows that the predicted dimensionless length (with respect to H_d) of the flow separation, x_s, and reattachment, x_r and x_{rs}, on the upper and lower walls are within 7% difference with MHFS measurements. One can note, however, that the numerical results included in Table 1 were computed assuming a fullydeveloped laminar flow up to the step, which does not correspond to physical reality.

5. CONCLUSIONS

An experimental and numerical investigation of air flow over a two-dimensional backward-facing step was carried out at selected laminar and transitional flow regimes and expansion ratios of 1·17 and 2·0. The results show that, by the use of multiple hot-film sensor (MHFS) arrays operated with a bank of constant-temperature anemometers, the locations of flow separation and reattachment points on the upper and lower walls of the two-dimensional channel can be obtained both nonintrusively and simultaneously. The MHFS measurements were found to be in good agreement with the present numerical predictions as well as with previous results. This MHFS measurement capability will provide a practical means for the characterization and manipulation of unsteady flow phenomena. However, development of MHFS arrays capable of detecting turbulent flow separation is greatly needed.

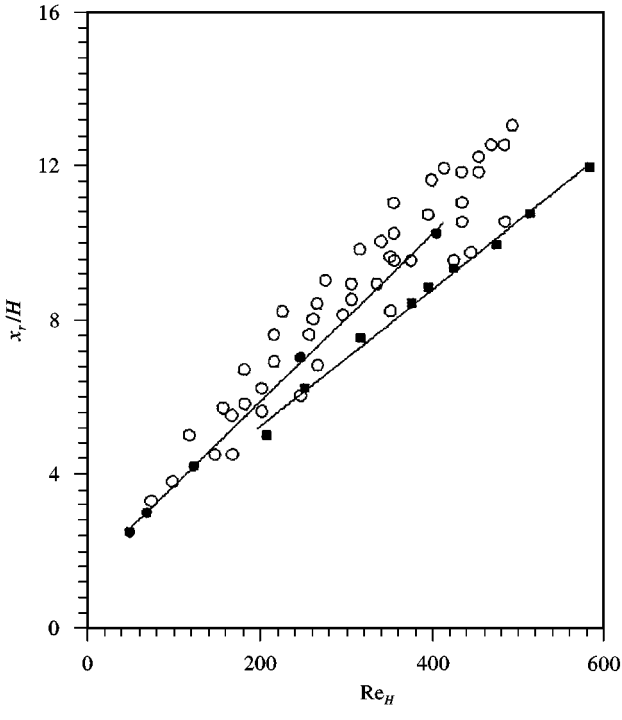

Figure 8. Variation of x_r with Re_H for ER = 1·17. ■, MHFS measurements; ○, Goldstein *et al.* (1970); ●, Armaly *et al.* (1983).

ACKNOWLEDGEMENTS

This work was supported by the Natural Sciences and Engineering Research Council of Canada. Mrs Y. Grunberg and T. Cholat are thanked for their help with the design and fabrication of the flow facility. The reviewer's valuable comments are also greatly appreciated.

References

Abbot, D. E. & Kline, S. J. 1962 Experimental investigations of subsonic turbulent flow over single and double backward-facing steps. *ASME Journal of Basic Engineering* **84,** 317–325.

Adams, E. W. & Johnston, J. P. 1988 Effects of the separating shear layer on the reattachment flow structure. Part 2: Reattachment length and wall shear stress. *Experiments in Fluids* **6,** 493–499.

Alfresson, P. H., Johansson, A. V., Haritonidis, J. H. & Eckelmann, H. 1988 The fluctuating wall-shear stress and the velocity field in the viscous sublayer. *Physics of Fluids* **31,** 1026–1033.

Armaly, B. F., Durst, F., Pereira, J. C. F. & Schonung, B. 1983 Experimental and theoretical investigation of backward-facing step flow. *Journal of Fluid Mechanics* **127,** 473–496.

Back, L. H. & Roshko, E. J. 1972 Shear-layer flow regions and wave instabilities and reattachment lengths downstream of an abrupt circular channel expansion. *Journal of Applied Mechanics* **39,** 677–781.

Benocci, C., Bellomi, P. & Michelassi, V. 1987 Comparison of cartesian and curvilinear grids for incompressible flow around steps. In *Numerical Methods in Laminar and Turbulent Flow*, pp. 584–594. White Plains, NY: Pineridge Press.

Bhatia, J. C., Hefner, J. N. & Jovanovic, J. 1982 Corrections of hot-wire anemometer measurements near walls. *Journal of Fluid Mechanics* **122,** 411–431.

Cherdron, W., Durst, F. & Whitelaw, J. H. 1978 Asymmetric flows and instabilities in symmetric ducts with sudden expansions. *Journal of Fluid Mechanics* **84,** 13–31.

Cook, W. 1991 Response of hot element wall shear stress gages in unsteady turbulent flows. *AIAA Paper* 91–0167.

Diller, T. E. & Telionis, D. P. 1989 Time-resolved heat transfer and skin friction measurements in unsteady flow. In *Advances in Fluid Mechanics Measurements* (ed. M. Gad-el-Hak), pp. 321–355.

Eaton, J. K., Jeans, A. H., Ashjaee, J. & Johnston, J. P. 1979 A wall-flow-direction probe for use in separating and reattaching flows. *ASME Journal of Fluids Engineering* **101,** 364–366.

Eaton, J. K. & Johnston, J. P. 1981 A review of research on subsonic turbulent flow reattachment. *AIAA Journal* **19,** 1093–1100.

Gartling, D. K. 1990 A test problem for outflow boundary conditions—flow over a backward-facing step. *International Journal of Numerical Methods in Fluids* **11,** 953–967.

Goldstein, R. J., Eriksen, V. L., Olson, R. M. & Eckert, E. R. G. 1970 Laminar separation, reattachment and transition of the flow over a downstream-facing step. *ASME Journal of Basic Engineering* **92,** 732–741.

Hussain, A. K. M. F. & Reynolds, W. C. 1975 Measurements in fully developed turbulent channel flow. *ASME Journal of Fluids Engineering* **97,** 568–578.

Kim, J. & Moin, P. 1985 Application of a fractional-step method to incompressible Navier-Stokes equations. *Journal of Computational Physics* **59,** 308–323.

Lee, T. & Basu, S. 1997 Nonintrusive measurement of boundary layers developing on a single and two circular cylinders. *Experiments in Fluids* **23,** 187–192.

Lee, T. & Budwig, R. 1991 Two improved methods for low-speed hot-wire calibration. *Measurement Science and Technology* **2,** 643–646.

Lorber, P. F., Carta, F. O. & Covino, A. F. 1992 An oscillating three-dimensional wing experiment: compressibility, sweep, rate, and geometry effects on unsteady separation and dynamic stall. United Technologies Research Center Rept. R92-958325-6, East Hartford, Connecticut, U.S.A.

Mateescu, D., Païdoussis, M. P. & Bélanger, F. 1994 A time-integration method using artificial compressibility for unsteady viscous flows. *Journal of Sound and Vibration* **177,** 197–205.

Nakayama, A., Stack, J. P., Lin, C. P. & Valareza, W. O. 1993 Surface hot-film technique for measurements of transition, separation, and reattachment points. AIAA Paper 93-2918.

Stack, J. P., Berry, S. A. & Mangalam, S. M. 1987 A unique measurement technique to study laminar-separation bubble characteristics on an airfoil. AIAA Paper 87-1271.

Sohn, J. 1988 Evaluation of FIDAP on some classical laminar and turbulent benchmarks. *International Journal of Numerical Methods in Fluids* **8,** 1469–1490.

Turan, O. & Azad, D. S. 1987 Wall effects on the hot-wire signal without flow. *Journal of Physics E: Scientific Instruments* **20,** 1278.

Vogel, J. C. & Eaton, J. K. 1985 Combined heat transfer and fluid dynamic measurements downstream of a backward-facing step. *ASME Journal of Fluids Engineering* **107,** 922–929.

Westphal, R. V., Eaton, J. K. & Johnston, J. P., 1981 A new probe for measurement of velocity and wall shear stress in unsteady reversing flow. *ASME Journal of Fluids Engineering* **103,** 478–482.

Westphal, R. V. & Johnston, J. P. 1984 Effect of initial conditions on turbulent reattachment downstream of a backward-facing step. *AIAA Journal* **22,** 1727–1731.